June 2005

Assembly of multicellular constructs and microarrays of cells using magnetic nanowires

Monica Tanase
Johns Hopkins University

Edward J. Felton
Johns Hopkins University

Darren S. Gray
Johns Hopkins University

Anne Hultgren
Johns Hopkins University

Christopher S. Chen
University of Pennsylvania, chrischen@seas.upenn.edu

See next page for additional authors

Assembly of multicellular constructs and microarrays of cells using magnetic nanowires

Abstract
An approach is described for controlling the spatial organization of mammalian cells using ferromagnetic nanowires in conjunction with patterned micromagnet arrays. The nanowires are fabricated by electrodeposition in nanoporous templates, which allows for precise control of their size and magnetic properties. The high aspect ratio and large remanent magnetization of the nanowires enable suspensions of cells bound to Ni nanowires to be controlled with low magnetic fields. This was used to produce one- and two-dimensional field-tuned patterning of suspended 3T3 mouse fibroblasts. Self-assembled one-dimensional chains of cells were obtained through manipulation of the wires' dipolar interactions. Ordered patterns of individual cells in two dimensions were formed through trapping onto magnetic microarrays of ellipsoidal permalloy micromagnets. Cell chains were formed on the arrays by varying the spacing between the micromagnets or the strength of fluid flow over the arrays. The positioning of cells on the array was further controlled by varying the direction of an external magnetic field. These results demonstrate the possibility of using magnetic nanowires to organize cells.

 Reprinted from *Lab on a Chip*, Volume 5, Issue 6, June 2005, pages 598-605.

Author(s)
Monica Tanase, Edward J. Felton, Darren S. Gray, Anne Hultgren, Christopher S. Chen, and Daniel H. Reich

Assembly of multicellular constructs and microarrays of cells using magnetic nanowires

Monica Tanase,†[a] Edward J. Felton,[a] Darren S. Gray,[b] Anne Hultgren,[a] Christopher S. Chen[c] and Daniel H. Reich*[a]

Received 17th January 2005, Accepted 21st April 2005
First published as an Advance Article on the web 13th May 2005
DOI: 10.1039/b500243e

An approach is described for controlling the spatial organization of mammalian cells using ferromagnetic nanowires in conjunction with patterned micromagnet arrays. The nanowires are fabricated by electrodeposition in nanoporous templates, which allows for precise control of their size and magnetic properties. The high aspect ratio and large remanent magnetization of the nanowires enable suspensions of cells bound to Ni nanowires to be controlled with low magnetic fields. This was used to produce one- and two-dimensional field-tuned patterning of suspended 3T3 mouse fibroblasts. Self-assembled one-dimensional chains of cells were obtained through manipulation of the wires' dipolar interactions. Ordered patterns of individual cells in two dimensions were formed through trapping onto magnetic microarrays of ellipsoidal permalloy micromagnets. Cell chains were formed on the arrays by varying the spacing between the micromagnets or the strength of fluid flow over the arrays. The positioning of cells on the array was further controlled by varying the direction of an external magnetic field. These results demonstrate the possibility of using magnetic nanowires to organize cells.

1. Introduction

The ability to create ordered arrangements of living cells on micropatterned surfaces is a rapidly developing technique in biology and biotechnology with applications including biosensing,[1–3] the study of mechanotransduction[4,5] and the exploration of the biochemistry of cell adhesion.[6–10] Current approaches to organize and pattern cells fall into two categories. First are passive techniques that rely purely on cell-surface interactions, in which substrates patterned with cell-adhesive ligands capture cells into desired patterns.[11–13] The effectiveness of this method depends on the natural cell adhesion process, which is slow, difficult to trigger or reverse, and can be different for different cell types. Thus, certain classes of cell patterns can be difficult to obtain.

In the second approach, active manipulation, a force is applied to suspended cells to direct them to the desired locations. These techniques are governed by the shorter timescales associated with physical transport of the cells, and are more easily reversible. Optical tweezers can be used to manipulate single cells,[14] and large numbers of cells can be positioned *via* dielectrophoretic trapping, wherein strong AC electric fields from shaped electrodes produce forces by coupling to the induced electric dipole moments of the cells.[15–18] However, this latter technique is complicated by the need to use a low-conductivity culture medium, and the necessity of working at high frequencies to avoid harmful effects such as charging of the cell membrane.

An alternative approach to active cell manipulation is to use magnetic fields and forces. While this requires the binding of magnetic particles to the cells, it has the advantages that low-frequency magnetic fields are not screened by culture media, and that there are no known short-term adverse effects on cells due to brief exposure to magnetic fields in the sub-Tesla range. This approach is now standard practice in magnetic cell separation,[19] typically making use of micron-size superparamagnetic beads.[20] Magnetic beads have also been used to apply localized forces to adherent cells to investigate cells' mechanical properties[21–24] and their functional response to force and stress.[25,26] For magnetic positioning, one can take advantage of the interactions of magnetic particles with both external magnetic fields and local fields generated by micropatterned features on the substrate. Controlled localization of ensembles of magnetic beads has been demonstrated using permanent magnet microarrays[27] and microelectromagnets,[28–30] and the latter technique has recently been used to move individual cells.[31] In this paper we introduce ferromagnetic nanowires as magnetic carrier particles for precision cell manipulation, and demonstrate their use with micromagnet arrays for cell localization, single-cell trapping, and ordered assembly.

A particle with magnetic moment $\boldsymbol{\mu}$, placed in a magnetic field $\boldsymbol{B}$, has energy $U = -\boldsymbol{\mu} \cdot \boldsymbol{B}$ and experiences a torque $\boldsymbol{\tau} = \boldsymbol{\mu} \times \boldsymbol{B}$. If the field is inhomogeneous, it also experiences a force proportional to the field gradient $\boldsymbol{F} = (\boldsymbol{\mu} \cdot \nabla)\boldsymbol{B}$. A magnetic particle suspended in a fluid will therefore rotate to align its moment parallel to the local field, and move towards regions of higher field to minimize its magnetic energy. Micrometer-scale magnetic structures can generate very large field gradients, and the forces they exert on magnetic particles can be used to position and collect the particles. However, both the

† Current address: Department of Biological Sciences, Columbia University, New York, NY 11027.
*reich@jhu.edu

fields and gradients from these structures fall off rapidly over distances comparable to their linear dimensions, and the force they can exert decreases with the separation r as $1/r^4$ at large distances. Therefore, to increase the range and effectiveness of such magnetic interactions, we use magnetic nanowires with large permanent magnetic moments that respond even to the weak fields far away from the micromagnets. These nanowires[32] are high aspect ratio ferromagnetic metal cylinders fabricated by electrochemical deposition in nanoporous templates.[33] The Ni wires used in this study, with diameter 350 nm and lengths in the range 15–30 μm, have been shown to outperform paramagnetic beads in conventional magnetic cell separation experiments.[34] They have permanent magnetic moments per unit length $\mu/L \sim 3 \times 10^{-14}$ A m^2 μm^{-1} directed along their long axis, and hence they are readily oriented and manipulated in small magnetic fields.[35–37] Their moment is typically 15 times the maximum moment of a superparamagnetic bead of comparable volume, and 200 times the bead's moment in a 10 mT field.[34] We use these nanowires with arrays of micromagnets to assemble cells bound to wires in a variety of ordered geometries, including patterns of single cells, pairs, lines, and stripes. Concurrently, we demonstrate how ordered structures such as chains of cells can be assembled through wire–wire interactions, both in the presence and absence of the arrays. We show that external fields can be used to tune and control the cells' interactions with the arrays, and that in combination with a simple fluidics apparatus, efficient and flexible cell positioning is obtained.

2. Experimental

Sample fabrication

Nickel nanowires were fabricated by electrochemical deposition in the cylindrical nanopores of 50 μm-thick alumina membranes (Anodisc, Whatman, Inc.) as described previously.[35] The wires' radius $r_W = 175 \pm 20$ nm was determined by the pore size, and their length was controlled by monitoring the deposition current. After deposition, the alumina was dissolved in 50 °C KOH, releasing the nanowires from the membranes. Once in suspension, the wires were collected with a magnet, washed with deionized water until the pH was neutral, sterilized in 70% ethanol, and suspended in 1X phosphate buffered saline solution (PBS). In the course of this process the wires were exposed to magnetic fields in excess of 0.3 T. Due to their large magnetic shape anisotropy, they subsequently remained highly magnetized with a remanent magnetization $M_W \approx 330$ kA m^{-1}, which is 70% of their saturation magnetization.[34] A scanning electron micrograph of several wires is shown in Fig. 1(a), and a close-up of a portion of a single wire is shown in Fig. 1(b).

For magnetic cell trapping, arrays of permalloy (Py, $Ni_{71}Fe_{29}$) micromagnets were fabricated on glass substrates. Py films 400 nm thick were deposited by magnetron sputtering, and the micromagnets were produced by contact photolithography and chemical etching in 10%wt. nitric acid. The individual micromagnets were elliptical in shape, with major axis $\alpha = 80$ μm, and minor axis $\beta = 8$ μm. This shape gives well-localized magnetic poles at the ends of the ellipses. Rectangular arrays containing up to 4000 ellipses were fabricated in 5 × 5 mm^2 fields. The center-to-center spacings between elements of the arrays were in the range 110 μm $\leqslant a \leqslant$ 340 μm in the direction parallel to the ellipses' major axes, and 17 μm $\leqslant b \leqslant$ 100 μm along their minor axes. Magnetization curves of the micromagnet arrays were measured in a vibrating sample magnetometer. In the 10 mT fields used in the trapping experiments, the ellipses have magnetization $M_E = 650$ kA m^{-1}, and magnetic moment $\mu_E = 1.3 \times 10^{-10}$ A m^2 per ellipse.

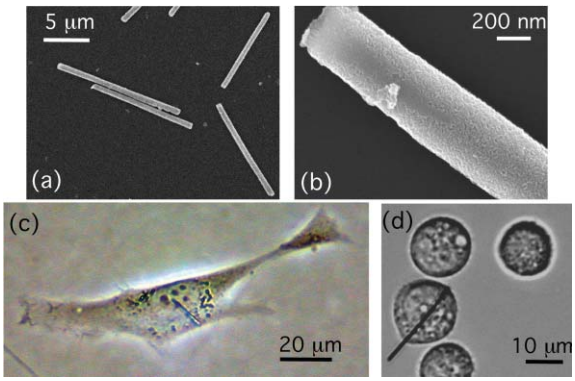

Fig. 1 (a) and (b) Scanning electron micrographs of nickel nanowires 350 nm in diameter. (c) A 15 μm Ni nanowire bound to a 3T3 mouse fibroblast cell after 24 h co-incubation. (d) Suspended 3T3 cells, with one bound to a 20 μm Ni nanowire.

Cell culture

NIH-3T3 mouse fibroblasts cells (ATCC, USA) were cultured at 37 °C, 5% CO_2 in Dulbecco's Modified Eagle Medium (DMEM) (Gibco Life Sciences) supplemented with 1% penicillin/streptomycin and 5% calf serum. The nanowires were introduced into the culture dishes when the cells were at 40% confluence at concentrations of at most 1 wire per 3 cells (1.5×10^4 wires ml^{-1}) to reduce the probability of multiple wires binding to the same cell. The wires were introduced in two aliquots, 30 min apart, with a 1 mT field applied throughout to reduce wire–wire interactions during this process. The extracellular matrix (ECM) proteins present in the serum-enriched media adsorbed to the hydrophilic native oxide layer on the surface of the wires, and the cells bound to the wires *via* integrins.[38] The wires and cells were incubated together for 24 h, at which point the wires have been shown to be internalized by the cells *via* integrin-mediated phagocytosis,[38] and the number of unbound nanowires was observed to be minimal. Fig. 1(c) shows a nickel nanowire bound to a 3T3 cell in culture. Previous studies have shown that Ni nanowires do not have toxic effects on 3T3 cells over periods longer than the duration of the current experiments.[38,39]

Magnetic manipulation of cells

For the magnetic manipulation experiments the cells were detached from the culture dishes using 0.25% trypsin and 1 mM EDTA in PBS, and re-suspended in fresh culture medium. The wire-cell binding is quite robust, and is resilient to the exposure to trypsin.[38,39] Cells without wires were removed by a single-pass magnetic separation[34] to increase the fraction of cells

bound to a wire to 75%. Of the cells with wires, approximately 10% were found to have more than one wire bound to them, but their behavior did not differ qualitatively from the cells with only one wire. A suspended 3T3 cell with a bound wire is shown in Fig. 1(d).

For the cell chaining experiments, 1 ml aliquots of cell suspensions with number densities in the range 1×10^5–2.5×10^5 cells ml^{-1} were placed in 1.8 cm^2 rectangular culture dishes. A uniform external field $B = 2$ mT was applied to align the wires, as shown schematically in Fig. 2(a), and chain formation was monitored as the cells settled to the bottom of the dish (Fig. 2(b)).

The cell trapping experiments were carried out either by sedimentation onto the micromagnet arrays under similar conditions as for the chaining experiments, or using a fluidics apparatus based on previously reported designs.[17,18] For this flow-assisted trapping, a microscope slide patterned with micromagnet arrays formed the bottom of a parallel-plate flow chamber with width $w = 6$ mm, height $t = 100$ μm, and length $L_C = 2.5$ cm. The arrays were oriented with the micromagnets' long axes perpendicular to the flow direction. The chamber's inlet and outlet ports were connected through multi-port valves to 10 ml syringes, which served as fluid reservoirs. The chamber was sterilized with 70% ethanol, and rinsed with DI water and culture medium before introduction of cells. Cell suspensions with number densities of 1×10^4–1×10^5 cells ml^{-1} were introduced at constant flow rates Q_F in the range $0.5 \leqslant Q_F \leqslant 7.5$ μL s^{-1} using an injection/withdrawal syringe pump (Model M362, Thermo Orion). A uniform external field $B = 10$ mT was applied parallel to the micromagnets' long axis. This field both magnetized the micromagnets, and aligned the wires with their moments parallel to that of the micromagnets.

Trapping and chain formation were recorded in phase contrast and bright field with the X10 and X40 objectives of a Nikon Eclipse TS100 inverted microscope equipped with a digital camera (Nikon Coolpix 995E) and video acquisition system. Higher-resolution phase contrast images of single cells with wires (Fig. 1) were obtained with the X20 objective of a Nikon TE2000 microscope, and reflected light images of cells trapped on top of micromagnets were taken with the X10 objective of a Nikon Labphot upright microscope.

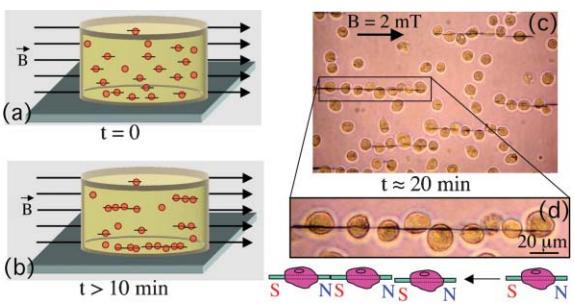

Fig. 2 Magnetic cell chaining. (a) Schematic of nanowires bound to suspended cells and aligned in a magnetic field $\boldsymbol{B}$. (b) Schematic of chain formation process due to magnetic dipole–dipole interactions between pre-aligned nanowires. (c) Cell chains formed on the bottom of a culture dish with $\boldsymbol{B} = 2$ mT. (d) Close up of a single cell chain detailing wire–wire alignment. Interactions of North and South poles of adjacent wires are indicated schematically below.

3. Results and discussion

Nickel nanowires were fabricated by electrodeposition with radius $r_W = 175 \pm 20$ nm, and lengths between 15 and 30 μm (Fig. 1(a)–(b)). The wires were then washed, coated with ECM proteins, and exposed to cells for 24 h (Fig. 1(c)). The cells were then detatched from their substrates for experimentation (Fig. 1(d)).

Chain formation

Fig. 2 shows the self-assembly of cells into chains. Here, an external field aligned the wires parallel to each other, as sketched in Fig. 2(a) and 2(b). The cells descended through the culture medium with a velocity of approximately 6–10 mm h^{-1}, and the nanowires experienced mutually attractive dipole–dipole forces due to the interactions of their magnetic moments. The alignment of the wires' moments made it unfavorable for wires to approach each other side by side, and instead favored the formation of head-to-tail chains, where the North pole of one wire abuts the South pole of the next. Chains of cells became detectable approximately 10 min into the experiment. As shown in Fig. 2(c), these formations can encompass many cells, and extend over hundreds of micrometers. Cells without wires settled at random. We observed two mechanisms of chain formation: aggregation in suspension, which leads to short chains, and the addition of descending cells or short chains to pre-existing chains on the chamber bottom. The chaining process ceased once all cells settled because the interwire forces were not sufficiently strong to move the 3T3 cells along the substrate.

Magnetic trapping

When cells with wires were brought close to the micromagnet arrays, either by sedimentation or by fluid flow, they were attracted to the ends of the micromagnets where the local field is most intense. This is shown in Fig. 3(a), where 3T3 cells have been trapped at the ends of six ellipses. Cell concentrations in the range 1×10^4–1×10^5 cells ml^{-1} were explored. The trapping efficiency increased with increasing cell concentration, but at the higher concentrations, significant clumping and/or chaining was observed in suspension prior to trapping. The optimum balancing between these two effects was found at 2.5×10^4 cells ml^{-1}, and the results presented herein are for this concentration.

We calculated the magnetic forces driving the cell trapping from the magnetostatic interactions between the wires and the micromagnet arrays. All calculations were done for the dominant case of one wire per cell. As the 10 mT external field oriented the wires nearly parallel to the ellipses' major axis, the force on a wire due to a single ellipse was $F_l = -\int_{\text{wire}} (\nabla B_E^x) \mathrm{d}\mu_w$. B_E^x is the component of the ellipse's magnetic field parallel to the wire, and $\mathrm{d}\mu_w = M_w \mathrm{d}V$ is the dipole moment of a volume element $\mathrm{d}V$ of the wire. Sufficient accuracy was obtained by treating the wires as one-dimensional objects with moment per unit length $\pi r_w^2 M_w$. B_E^x and ∇B_E^x were calculated from

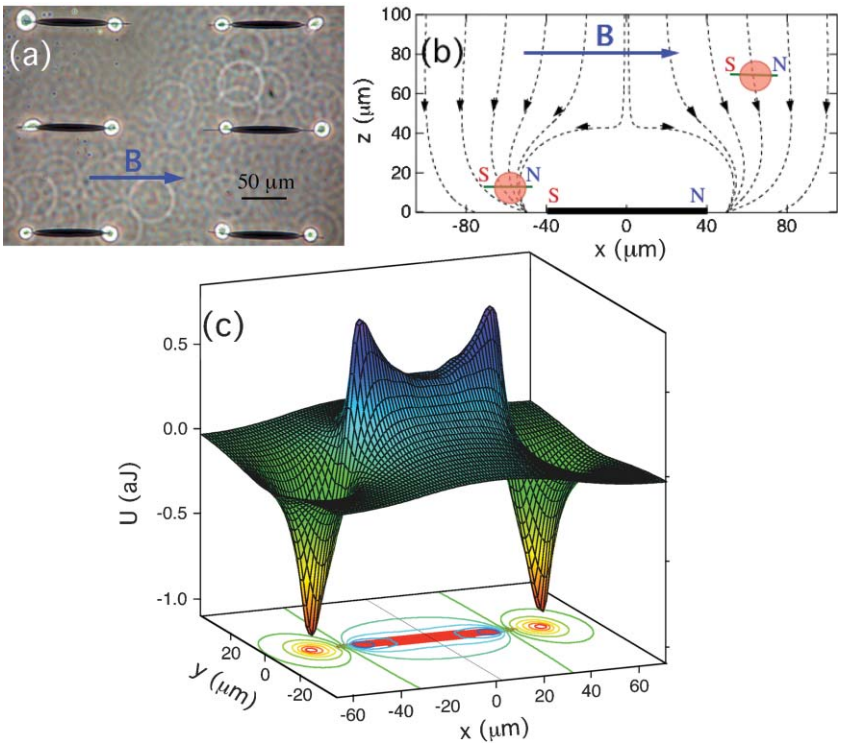

Fig. 3 (a) Trapping of single cells by ellipsoidal micromagnets. Aligning field $B = 2$ mT. (b) Calculated settling trajectories for a spherical cell with density 1.08 g cm^{-3} over the centerline of one of the ellipses in (a). (c) Calculated wire–ellipse interaction energy U_1 at a wire height $z = 3$ μm. Ellipse footprint is shown in red on floor of the figure.

the bound surface current density on the ellipse using the Biot–Savart law. $\boldsymbol{F}_1$ was computed numerically on a 0.5 μm mesh, and the total magnetic force $\boldsymbol{F}_M$ on a wire at position $\boldsymbol{r}$ above an array was obtained to better than 0.1% accuracy *via* interpolation of the computed values of $\boldsymbol{F}_1$ as $\boldsymbol{F}_M(\boldsymbol{r}) = \sum_{n,m} \boldsymbol{F}_1(\boldsymbol{r} - \boldsymbol{R}_{n,m})$, where $\boldsymbol{R}_{n,m} = na\hat{x} + mb\hat{y}$ gives the positions of the micromagnets in the arrays.

Fig. 3(b) displays sedimentation trajectories calculated for a cell with a wire settling over the centerline of an isolated micromagnet. As all motion in these experiments occured at low Reynolds number, the velocity field that determines these trajectories is $\boldsymbol{v} = \boldsymbol{F}_T/\zeta$, where ζ is the appropriate drag coefficient, and $\boldsymbol{F}_T$ includes both magnetic and gravitational forces. Those shown were calculated for a 16 μm diameter spherical cell bound to a 20 μm wire. The concentration of the trajectories illustrates the attractive action of the trap. Note the region extending approximately 40 μm above the micromagnet from which cells with wires are excluded. Such calculations are in good agreement with the observed motion of the cells.

The magnetic energy $U(\boldsymbol{r})$ of a nanowire over an array is useful in visualizing how the cells with wires are trapped on the arrays. This was calculated from $U(\boldsymbol{r}) = \sum_{n,m} U_1(\boldsymbol{r} - \boldsymbol{R}_{n,m})$, where $U_1 = -\int_{\text{wire}} B_E^x \mathrm{d}\mu_w$ is the energy of a wire interacting with a single ellipse. A map of U_1 with a nanowire at height $z = 3$ μm above the substrate is shown in Fig. 3(c). Note the repulsive region with $U_1 > 0$ located over the ellipse, and the deep, attractive wells with $U_1 < 0$ at each end of the ellipse. These calculations demonstrate an important feature of the trapping, namely that with $\boldsymbol{\mu}_W \| \boldsymbol{\mu}_E$ the cells with wires are strongly repelled from the centers of the micromagnets and never land there.

Flow-assisted trapping

The trapping efficiency and speed were increased significantly when using fluid flow to bring the cells onto the arrays. Some of the cell patterns achieved with flow-assisted trapping are shown in Fig. 4. Fig. 4(a) shows a sparse array where the predominant mode of trapping is the capture of single cells, as is shown in more detail in Fig. 4(d). The array in Fig. 4(b) contains well-separated columns of closely spaced ellipses. A close-up of this array is shown in Fig. 4(e). Here, the trapping process induced formation of lines of cells along the edges of the columns. The spaces between the columns were swept clear of cells by the fluid flow. Fig. 4(c) and the corresponding high-magnification image in Fig. 4(f) show that when columns such as those in Fig. 4(b) were placed into close proximity, sharply defined stripes of cells are formed. Formation of these patterns depended critically on the repulsion of cells with wires from the regions directly over the micromagnets. Cells without wires were removed from all types of arrays by the fluid flow. As can be seen in Figs. 4(d)–(f), all of the trapped cells had wires.

As the cells approached the array, the large-scale features of the cell pattern were determined by the field profile sensed by the nanowires well above the substrate. The grayscale magnetic energy maps in Figs. 4(g)–(i) correspond to the regions of the arrays shown in Figs. 4(d)–(f), and were calculated for a wire

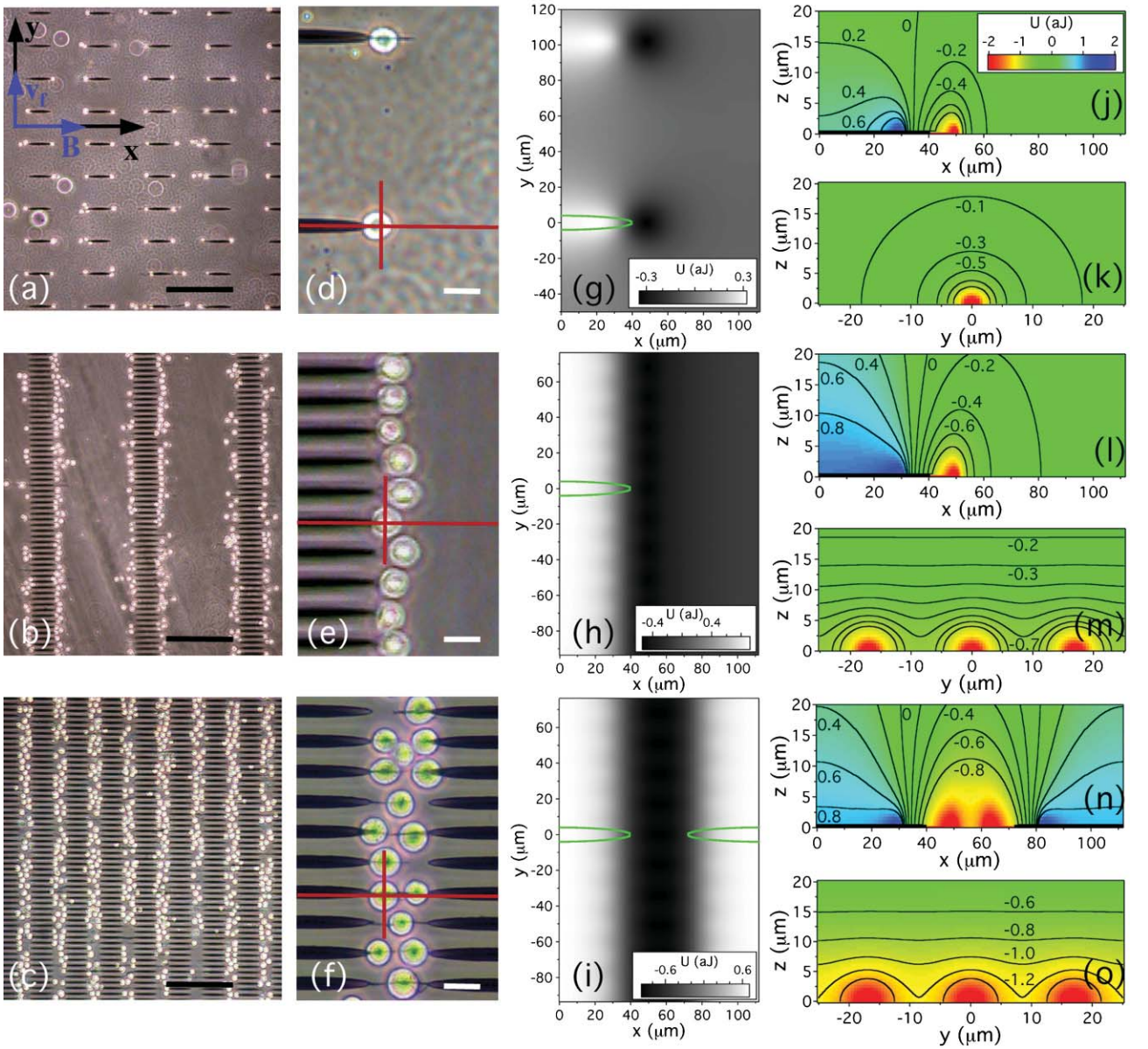

Fig. 4 (a)–(c) Overview images of cell trapping on magnetic arrays. The direction of the external field $B = 10$ mT and the fluid flow $Q_f = 1.7$ μL s^{-1} are shown in (a). The array lattice parameters are (a) $a = 125$ μm, $b = 100$ μm; (b) $a = 260$ μm, $b = 17$ μm; (c) $a = 32$ μm, $b = 17$ μm. Scale bars in (a)–(c) = 200 μm. (d)–(f) Close-up images of panels (a)–(c). Scale bars in (d)–(f) = 20 μm. (g)–(i) Calculated magnetic energy for a cell with a wire at a height $z = 8$ μm above the regions shown in (d)–(f). The wire is attracted to dark regions, and repelled from white regions. Selected micromagnets are outlined in green. (j)–(o) Calculated magnetic energy of wire and cell in vertical planes above the red lines in (d)–(f). The micromagnets appear as thick black lines at the bottom of (j), (l), and (n). Trapping regions appear in red.

of length $L = 20$ μm at height $z = 8$ μm above the substrate, a distance equal to the average suspended cell radius. At this height, in the sparse arrays, the attractive wells with $U < 0$ from the individual ellipses, are well separated, and have sizes comparable to a single cell. The wells appear as dark spots in Fig. 4(g). In the denser arrays, however, the wells overlap and reinforce each other, forming regions resembling trenches running parallel to the columns of ellipses that attract the wires more strongly than do the individual ellipses. For widely separated columns the trenches are narrow as in Fig. 4(h), leading to the capture of lines of cells as seen in Fig. 4(e), while for close-packed columns the trenches are wider, as in Fig. 4(i), and stripes of cells form such as those in Fig. 4(f). Note also that the regions (shown in white) with $U > 0$ over the ellipses coalesce over the columns in Figs. 4(h) and 4(i), leading to large areas of the arrays from which the cells are repelled and are pushed toward the regions where trapping is favored. Indeed the dense arrays are more efficient at trapping cells, as they always subject a cell with a wire to either attractive or repulsive interactions, whereas on the sparse arrays there are large low-force regions that do not significantly perturb the cells' motion due to the flow.

Figs. 4(j)–(o) show color-coded magnetic energy maps for 20 μm wires in the x–z and y–z planes above the horizontal and

vertical lines in Figs. 4(d)–(f). The x–z maps over the centerline of an ellipse show that there is a strongly localized binding site for a wire with its end just touching the end of the ellipse. The ellipses appear as black bars at the bottom of these figures. Note that the color scale has been truncated, and the calculated depths of the wells are $U_{\mathrm{Min}} = -6.4$ aJ, -6.6 aJ, and -7.1 aJ for Figs. 4(d)–(f), respectively. The y–z maps cut through these binding sites, and show that these sites are well localized at the tip of each ellipse. This shows that the final position of the cells within the attractive regions on the array is predominantly determined by the interaction of the wire with a single ellipse, and explains the registry of the cells within the trenches in Figs. 4(e) and 4(f). The repulsive regions (blue) extend to much higher altitude in the close-packed arrays, which contributes to their greater efficiency at trapping.

Once a cell was trapped at a micromagnet, subsequent cells were prevented from trapping at that location by volume exclusion. This contributed to the quasi-regular positioning of the cells in the lines and stripes shown in Figs. 4(d) and 4(g) respectively. At the same time, the presence of a trapped wire such as that in Fig. 5(a) modified the magnetic energy surface seen by subsequent cells with wires. This can be exploited to form cell chains similar to those described above, but lined up with the micromagnets, as shown in Figs. 5(b) and 5(c). The black line in Fig. 5(d) shows the calculated wire–ellipse interaction energy U_1 along an ellipse's centerline with distance from the end of the ellipse at $z = 0.4$ μm. A 20 μm wire trapped by this ellipse with its center at $x = 50$ μm produces a secondary energy minimum, as shown by the red curve in Fig. 5(d), which was calculated for the purposes of illustration for a second 20 μm wire at a height $\Delta z = 2r_{\mathrm{W}}$ above the first wire. The second wire in turn produces a new trapping site, shown in blue, that can capture a third wire-cell pair, leading to the situation shown in Fig. 5(c).

The length of these trapped chains can be controlled by the horizontal spacing between the micromagnets in the array. Fig. 5(e) shows a gap sized for trapping pairs of cells, and Fig. 5(f) shows a gap that yields chains of length four. Thus the micromagnets can serve as localized initiation sites for cell chain formation, with the spacing between the micromagnets controlling the number of cells in the chains.

Effects of fluid flow

The speed and direction of the fluid flow in the chamber further controls the geometry of the trapped cell patterns. The fluid force f_{F} on the cells affects both the trapping efficiency and the occurrence of chaining. The images shown in Figs. 3–5 were obtained at flow rates 0.5 μl s^{-1} $\leqslant Q_{\mathrm{F}} \leqslant$ 1.7 μl s^{-1}. These low flow rates favored high trapping site occupancy (>80%), as well as the formation of cell chains. Above $Q_{\mathrm{F}} \sim$ 1.7 μl s^{-1}, first chaining and then trapping were incrementally suppressed, and at the highest flow rate measured, $Q_{\mathrm{F}} = 7.5$ μl s^{-1}, chain formation was virtually absent, with only 10% of the sites occupied by cells. Since the trapping must overcome the fluid force on the cells, increasing f_{F} reduced the range of influence of the trapping sites, and raised the threshold for the magnetic force required to capture cells. From the hydrodynamic force on a sphere near a surface under laminar flow,[40,41] we obtain $f_{\mathrm{F}} \approx 1.5$ nN at $Q_{\mathrm{F}} = 7.5$ μl s^{-1}.[42] This is equal to the calculated peak wire–wire force F_{WW}, and explains the suppression of chain formation at higher flow rates. The peak wire–trap force $F_{\mathrm{Tr}} \approx 22$ nN considerably exceeds f_{F}, consistent with our observation that once a cell was trapped by a micromagnet, even our highest constant flow rates were not sufficient to remove it. Note, however, that by pulsing the inlet syringe briefly it was possible to dislodge all the cells from the traps, and thus the magnetic trapping process can indeed be made reversible.

The cell patterning could also be controlled by the direction of the flow relative to the arrays. When the flow was angled more than 5° from perpendicular to the long axes of the ellipses, we obtained strong preferential trapping on the upstream ends of the ellipses, as shown in Fig. 6. This occurs because the incoming cells were blocked from reaching the downstream trapping site of each by the repulsive region above the ellipse's center. The diagonal flow also ensured that most cells reached the proximity of a trapping site while traversing the array, and the trapping efficiency per upstream site was therefore increased over perpendicular flow. Compare Fig. 6(a) where 94% of the upstream sites and only 3% of the downstream sites are occupied, to Fig. 4(b) where under perpendicular flow, the overall occupancy rate is 78%. This selectivity was also observed in sparser arrays, as shown in Fig. 6(b) where 83% of the upstream sites were occupied, and

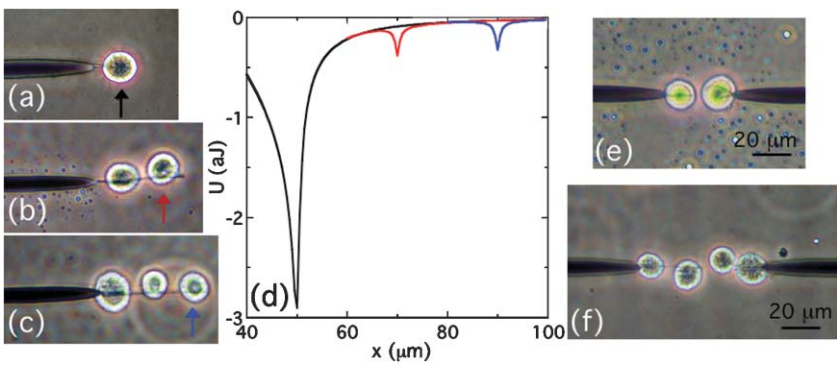

Fig. 5 Directed cell chain formation due to nanowire–nanowire interactions. (a)–(c) illustrate progressive growth of cell chains. (d) shows trapping potential along centerline of ellipse, with modified potential seen by second cell (red) and third cell (blue) due to previous cell. (e)–(f) Trapping with available space sized for two and four cells, respectively.

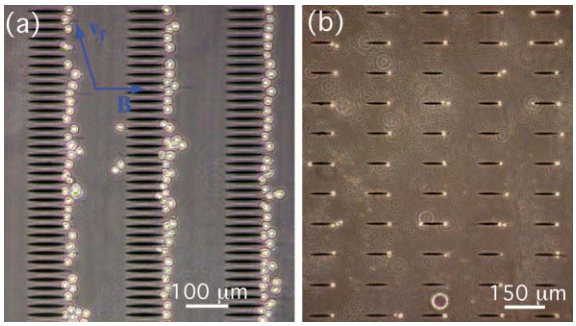

Fig. 6 Magnetic trapping under diagonal fluid flow at flow rates Q_f = 1.7 μL s^{-1} (a) and 5 μL s^{-1} (b), directed as shown. The array lattice parameters are (a) a = 200 μm, b = 120 μm; (b) a = 380 μm, b = 20 μm.

only 25% of the downstream sites. Note also the large number of single cells obtained on the sparse array: approximately 800 across a 5 × 5 mm^2 area in less than 10 minutes. This is potentially useful in applications that require the interrogation of spatially separated cells.

Effects of field reversal

Trapping experiments were also performed with the applied field anti-parallel rather than parallel to the magnetization direction of the micromagnets ($\boldsymbol{B} = -B\hat{\boldsymbol{x}}$). For fields less than the coercive field $\mu_0 H_C$ = 2 mT at which the micromagnets' moments reverse, the wires' moments were anti-parallel to those of the micromagnets, and the wire–micromagnet interaction changed sign.[43] The regions of attraction shifted from the tips of the ellipses to over their bodies, and cells with wires landed on top of the micromagnets, rather than at their ends. This is shown in Fig. 7(a), with B = −0.5 mT. Fig. 7(b) shows that the attractive wells in the x–y plane at z = 8 μm are now located over the columns of ellipses. There is a broad attractive region at lower altitude over the whole column, as shown in the x–z map along the centerline of one ellipse in Fig. 7(c), and in the y–z map over the center of a column shown in Fig. 7(d).

The anti-parallel trapping was less effective than the parallel trapping shown in Fig. 4, as the weaker modulation of the wire energy led to less well-defined trapping sites with weaker binding. This was further exacerbated by the low remanent magnetization of our Py ellipses which resulted in $M_E \approx$ 300 kA m^{-1} at B = −0.5 mT. The resulting weak magnetic forces placed an upper limit on the flow rate of $Q_F <$ 0.15 μl s^{-1} for effective trapping. Thus, while these experiments demonstrated the potential to trap cells on top of the ellipses, this approach could readily be improved by constructing the micromagnets from magnetically harder materials.

4. Conclusions

We have shown that magnetic nanowires used in conjunction with micropatterned magnetic arrays provide a flexible tool for manipulation and positioning of cells. While in this paper we have illustrated this technique with 3T3 cells, it is not restricted to a particular cell type, and we have observed similar effects using other cell lines, including HeLa and MCF10A breast cells.[44] Due to their large remanent magnetic moment, the nickel nanowires used are very responsive to small fields, even when bound to a cell. The nanowires were shown to mediate self-assembly of cell chains through dipole–dipole interactions. Trapping and positioning of cells bound to wires on arrays of patterned micromagnets was achieved using both sedimentation and fluid flow. This process can be precisely modeled based on magnetic interactions between the wires and the micromagnets, and therefore a wide variety of potentially useful geometries can be readily engineered. The magnetic cell patterning was shown to be controllable through a combination of external magnetic fields and fluid flow. In particular, the ability to invert the sign of the wire–micromagnet

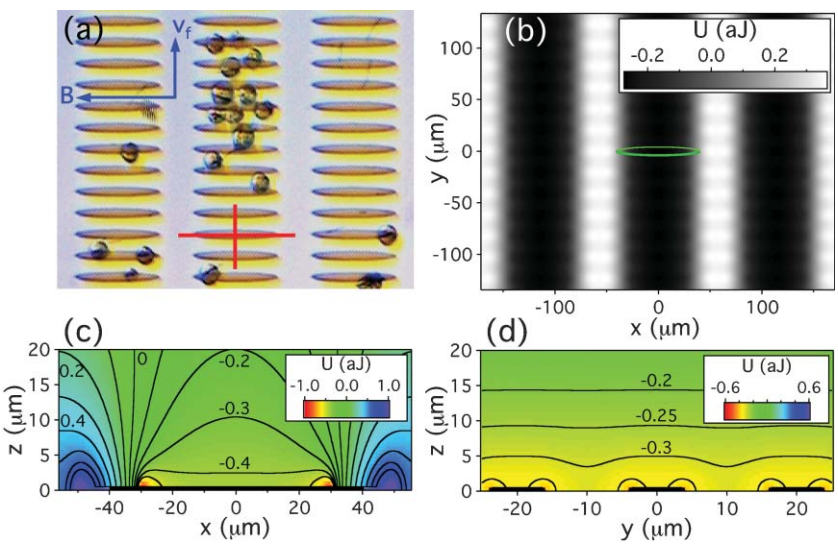

Fig. 7 (a) Magnetic trapping with the nanowires anti-aligned with the micromagnets' moments by reversing B. (b)) Calculated magnetic energy for a cell with a wire at a height z = 8 μm above the array shown in (a). The wire is attracted to dark regions, and repelled from white regions. One micromagnet in the array is outlined in green. (c)–(d) Calculated magnetic energy of a wire and cell in vertical planes above the red lines in (a). The micromagnets appear as thick black lines at the bottom of (c) and (d).

interaction at any time by reversing the external field direction has the potential to enable controlled assembly and spatial positioning of multiple cell types or other heterogenous configurations without the use of selective functionalization or other chemical modification of the substrate. If desired, the magnetic response of the nanowires can also potentially be enhanced by using magnetic materials stronger than Ni, such as Fe and Co and their alloys, although the stability of these structures in media, and their effects on cell viability will need to be fully explored. Ultimately, the ability to use magnetic nanowires to bring large numbers of cells to precise locations in a custom-engineered environment should enable their use in a variety of research, diagnostic and biosensing applications.

Acknowledgements

This work was supported by DARPA/AFOSR Grant No. F49620-02-1-0307, by the David and Lucile Packard Foundation through Grant No. 2001-17715, by NSF Grant No. DMR-0080031, and by the NIBIB (EB00262).

Monica Tanase,†[a] Edward J. Felton,[a] Darren S. Gray,[b] Anne Hultgren,[a] Christopher S. Chen[c] and Daniel H. Reich*[a]
[a]*Department of Physics and Astronomy, The Johns Hopkins University, Baltimore, MD 21218 E-mail: reich@jhu.edu*
[b]*Department of Biomedical Engineering, The Johns Hopkins University, Baltimore, MD 21205*
[c]*Department of Bioengineering, School of Engineering and Applied Science, University of Pennsylvania, Philadelphia, PA 19104*

References

1 J. J. Pancrazio, J. P. Whelan, D. A. Borkholder, W. Ma and D. A. Stenger, *Ann. Biomed. Eng.*, 1999, **27**, 697–711.
2 R. Kapur, *Ann. N. Y. Acad. Sci.*, 2002, **961**, 196–197.
3 A. M. Aravanis, B. D. DeBusschere, A. J. Chruscinsk, K. H. Gilchrist, B. K. Kobilka and G. T. Kovacs, *Biosens. Bioelectron.*, 2001, **16**, 571–577.
4 C. S. Chen, J. T. Tan and J. Tien, *Annu. Rev. Biomed. Eng.*, 2004, **6**, 275–302.
5 J. L. Tan, J. Tien, D. M. Pirone, D. S. Gray, K. Bhadriraju and C. S. Chen, *Proc. Natl. Acad. Sci. USA*, 2003, **100**, 1484–1489.
6 C. M. Nelson and C. S. Chen, *J. Cell Sci.*, 2003, **116**, 3571–3581.
7 C. M. Nelson, D. Pirone, J. L. Tan and C. S. Chen, *Mol. Biol. Cell*, 2004, **15**, 483–495.
8 M. Kato and M. Mrksich, *Biochemistry*, 2004, **43**, 2699–2707.
9 C. S. Chen, J. L. Alonso, E. Ostuni, G. M. Whitesides and D. E. Ingber, *Biochem. Biophys. Res. Commun.*, 2003, **307**, 355–361.
10 S. N. Bhatia, M. L. Yarmush and M. Toner, *J. Biomed. Mater. Res.*, 1997, **34**, 189–199.
11 C. Roberts, C. S. Chen, M. Mrksich, V. Martichonok, D. E. Ingber and G. M. Whitesides, *J. Am. Chem. Soc.*, 1998, **120**, 6548–6555.
12 R. Singhvi, A. Kumar, G. P. Lopez, G. N. Stephanopoulos, D. I. Wang, G. M. Whitesides and D. E. Ingber, *Science*, 1994, **254**, 696–698.
13 B. C. Wheeler, J. M. Corey, G. J. Brewer and D. W. Branch, *J. Biomech. Eng.*, 1999, **121**, 73–78.
14 D. Choquet, D. P. Felsenfeld and M. P. Sheetz, *Cell*, 1997, **88**, 39–48.
15 R. Pethig, *Crit. Rev. Biotechnol.*, 1996, **16**, 331–348.
16 R. Pethig and G. H. Markx, *Trends Biotechnol.*, 1997, **15**, 426–432.
17 J. Voldman, R. A. Braff, M. Toner, M. L. Gray and M. A. Schmidt, *Biophys. J.*, 2001, **80**, 531–541.
18 D. S. Gray, J. L. Tan, J. Voldman and C. S. Chen, unpublished work, 2003.
19 I. Safarik and M. Safaikova, *J. Chromatogr., B*, 1999, **722**, 33–53.
20 *Scientific and Clinical Applications of Magnetic Microspheres*, ed. U. Häfeli, W. Schütt, J. Teller and M. Zborowski, Plenum Press, New York, 1997.
21 F. C. MacKintosh and C. F. Schmidt, *Curr. Opin. Coll. Interface Sci.*, 1999, **4**, 300–307 and references therein.
22 A. R. Bausch, U. Hellerer, M. Essler, M. Aepfelbacher and E. Sackmann, *Biophys. J.*, 2001, **80**, 2649–2657.
23 B. D. Matthews, D. R. Overby, F. J. Alenghat, J. Karavitis, Y. Numaguchi, P. G. Allen and D. E. Ingber, *Biochem. Biophys. Res. Commun.*, 2004, **313**, 758–764.
24 B. Fabry, G. N. Maksym, J. P. Butler, M. Glogauer, D. Navajas and J. J. Fredberg, *Phys. Rev. Lett.*, 2001, **87**, 148102.
25 N. Wang, J. P. Butler and D. E. Ingber, *Science*, 1993, **260**, 5111, 1124–1127.
26 C. J. Meyer, F. J. Alenghat, P. Rim, J. H. Fong, B. Fabry and D. E. Ingber, *Nat. Cell Biol.*, 2000, **2**, 666–668.
27 B. B. Yellen and G. Friedman, *Langmuir*, 2004, **20**, 2553–2559.
28 T. Deng, G. M. Whitesides, M. Radhakrishnan, G. Zabow and M. Prentiss, *Appl. Phys. Lett.*, 2001, **78**, 1775–1777.
29 C. S. Lee, H. Lee and R. M. Westervelt, *Appl. Phys. Lett.*, 2001, **79**, 3308–3310.
30 A. Rida, V. Fernandez and M. A. M. Gijs, *Appl. Phys. Lett.*, 2003, **83**, 2396–2398.
31 H. Lee, A. M. Purdon and R. M. Westervelt, *Appl. Phys. Lett.*, 2004, **85**, 1063–1065.
32 T. M. Whitney, J. S. Jiang, P. C. Searson and C. L. Chien, *Science*, 1993, **261**, 1316–1319.
33 A. Fert and L. Piraux, *J. Magn. Magn. Mater.*, 1999, **200**, 338–358.
34 A. Hultgren, M. Tanase, C. S. Chen, G. J. Meyer and D. H. Reich, *J. Appl. Phys.*, 2003, **93**, 7554–7556.
35 M. Tanase, L. A. Bauer, A. Hultgren, D. M. Silevitch, L. Sun, D. H. Reich, P. C. Searson and G. J. Meyer, *Nanolett.*, 2001, **1**, 155–158.
36 M. Tanase, D. M. Silevitch, A. Hultgren, L. A. Bauer, P. C. Searson, G. J. Meyer and D. H. Reich, *J. Appl. Phys.*, 2002, **91**, 8549–8551.
37 C. L. Chien, L. Sun, M. Tanase, L. A. Bauer, A. Hultgren, D. M. Silevitch, G. J. Meyer, P. C. Searson and D. H. Reich, *J. Magn. Magn. Mater.*, 2002, **249**, 146–155.
38 A. Hultgren, M. Tanase, E. J. Felton, K. Bhadriraju, A. K. Salem, C. S. Chen and D. H. Reich, *Biotechnol. Prog.*, 2005, **21**, 509–515.
39 A. Hultgren, M. Tanase, C. S. Chen and D. H. Reich, *IEEE Trans. Magn.*, 2004, **40**, 2988–2990.
40 M. Chaoui and F. Feuillebois, *Q. J. Mech. Appl. Math.*, 2003, **56**, 381–410.
41 A. J. Goldman, R. G. Cox and H. Brenner, *Chem. Eng. Sci.*, 1967, **22**, 653–660.
42 For our flow velocities and chamber dimensions the flow field is laminar, and so the fluid force on a trapped cell can be estimated from the frictional force on a stationary sphere of radius b touching a wall in a linear shear flow $v = \kappa z$: $f_{\mathrm{Fluid}} = 6\pi\eta b^2\kappa C$, where $C \approx 1.7$.[40,41] Assuming an overall parabolic velocity profile $v(z) = \frac{6Q_{\mathrm{F}}}{wt^2} z\left(1 - {}^{z}/_{t}\right)$ gives $\kappa \approx \frac{6Q_{\mathrm{F}}}{wt^2}$, which with $\eta \approx 10^{-3}$ Pa s, yields 0.1 nN $\leqslant f_{\mathrm{Fluid}} \leqslant$ 1.5 nN for 0.5 μl $\mathrm{s}^{-1} \leqslant Q_F \leqslant$ 7.5 μl s^{-1}.
43 D. H. Reich, M. Tanase, A. Hultgren, L. A. Bauer, C. S. Chen and G. J. Meyer, *J. Appl. Phys.*, 2003, **93**, 7275–7280.
44 A. Hultgren, *PhD Thesis*, The Johns Hopkins University, Baltimore, MD, 2005.